



Adsorption of Ammonia from Aqueous Solutions by Using Activated Iron Scraps Particles

Omar Nasri Naji¹, Bashar Abdulazeez Mahmood^{1*}, Yasir Al-Ani²

¹ Department of Chemistry, College of Education for Pure Science, University of Anbar, Anbar 31001, Iraq

² Department of Dams & Water Resources, Engineering, Faculty of Engineering, University of Anbar, Anbar 31001, Iraq

Corresponding Author Email: esp.bashar.abdulaziz@uoanbar.edu.iq

Copyright: ©2025 The authors. This article is published by IIETA and is licensed under the CC BY 4.0 license (<http://creativecommons.org/licenses/by/4.0/>).

<https://doi.org/10.18280/iji.080408>

Received: 26 May 2025

Revised: 11 July 2025

Accepted: 22 August 2025

Available online: 31 August 2025

Keywords:

ammonia removal, adsorption, iron waste, RSM optimization, sustainable low-cost adsorbent aqueous solution treatment

ABSTRACT

Ammonia contamination in aquatic environments has become a major ecological and health concern. This study investigates the use of industrial iron waste, a low-cost and readily available material, as an adsorbent for removing ammonia from polluted water. Laboratory experiments were conducted to evaluate the effects of four key parameters: solution pH, contact time, adsorbent dosage, and initial ammonium concentration. Optimization was performed using Response Surface Methodology (RSM) in Design-Expert 7.1.6, and ANOVA confirmed that all variables significantly influenced adsorption efficiency. Surface characterization before and after activation revealed physicochemical enhancements. Adsorption equilibrium data were fitted to Langmuir and Freundlich isotherms. The Langmuir model showed a superior fit ($R^2 = 0.97$), indicating monolayer adsorption with a maximum capacity of 13.6 mg/g, while Freundlich results ($R^2 = 0.94$) also supported favorable multilayer adsorption. The study achieved high removal efficiencies of up to 94% under optimized conditions, underscoring the potential of industrial iron waste as an effective and sustainable adsorbent. Its low cost, ease of activation, and local abundance make it a promising candidate for scalable water treatment applications, particularly in resource-constrained areas.

1. INTRODUCTION

Ammonia contamination has become a major environmental and health concern in freshwater ecosystems worldwide. It originates primarily from anthropogenic activities such as agricultural runoff, municipal wastewater discharge, landfill leachate, and industrial effluents [1-3]. In aqueous environments, ammonia exists in a dynamic equilibrium between ammonium ions (NH_4^+) and unionized ammonia gas (NH_3). This equilibrium is highly dependent on water pH and temperature, where alkaline conditions favor the more toxic NH_3 form [4, 5]. Seasonal thermal stratification in reservoirs has also been shown to affect ammonia transformation dynamics and accumulation of toxic forms in bottom layers [2].

Excessive ammonia levels in water bodies can lead to eutrophication, oxygen depletion, and severe toxicity to aquatic organisms, especially fish and invertebrates. Moreover, the presence of free ammonia in drinking water supplies poses a direct risk to human health and challenges conventional disinfection processes [6, 7]. This necessitates the development of effective and adaptable treatment technologies that can perform well under diverse environmental conditions.

Traditional ammonia removal methods include air stripping [8], chlorination [9], biological nitrification-denitrification [10], and ion exchange [11]. However, these methods often involve high capital and operational costs, complex maintenance requirements, or limited effectiveness at low

concentrations [12, 13]. Adsorption has gained growing attention as a practical and efficient alternative, offering simplicity, low-cost operation, and minimal secondary pollution [14]. Its suitability for decentralized and small-scale treatment makes it ideal for resource-constrained regions [15].

A wide array of adsorbent materials has been investigated for ammonia removal, ranging from zeolites [16] and activated carbon [17] to biochars, agricultural residues [18], and clay minerals [19]. While many of these materials exhibit satisfactory performance, they often suffer from issues related to regeneration, cost, or inconsistent adsorption capacity [20]. In contrast, iron-based materials—especially industrial iron filings—have attracted increasing interest due to their wide availability, low cost, and strong chemical affinity toward various contaminants [21, 22]. These materials, commonly generated as waste during machining operations, offer magnetic properties and redox activity that facilitate pollutant removal through mechanisms such as ion exchange, surface complexation, and electrostatic attraction [23].

Numerous studies have reported the application of iron filings in the removal of heavy metals [24], phosphate [25], nitrate [26], and organic dyes [27] from contaminated water [28]. Furthermore, recent research has explored the potential of modifying these iron-based materials to enhance their surface area and reactivity. Techniques such as acid/base treatment [29], ultrasonic irradiation [30], and thermal processing [31] have proven effective in increasing porosity, exposing active sites, and introducing functional groups like

hydroxyl and iron oxides, which play key roles in adsorption interactions [32-34].

Importantly, the reuse of iron waste aligns with global sustainability goals and the principles of circular economy by converting industrial byproducts into valuable resources for environmental remediation [35]. Therefore, the development of activated iron-based adsorbents presents a sustainable, efficient, and scalable solution to address the challenge of ammonia pollution in water systems, particularly in areas where access to advanced treatment technologies is limited [36, 37]. Supporting this trend, Al-Ani et al. [38] successfully demonstrated the use of industrial iron scrap as a zero-valent iron source to remove up to 45% of color and 33% of COD from synthetic dyeing wastewater, further validating the versatility and environmental potential of iron-based materials for pollutant removal. Although materials such as natural zeolites and activated carbon have achieved effective ammonia removal, their high costs, regeneration challenges, and limited availability restrict broader application [39]. In contrast, industrial iron waste represents a locally available, low-cost, and sustainable alternative with enhanced redox activity and easier activation [40], highlighting the novel contribution of this study within the framework of circular water treatment technologies.

2. MATERIALS AND METHODS

2.1 Materials

2.1.1 Iron particles preparation

Iron waste particles were collected from local machining workshops in the form of industrial waste. This material was selected due to its abundance, low cost, and well-documented potential as an adsorbent for water treatment applications [41]. The raw filings were initially rinsed with deionized water several times to eliminate grease, dust, and oxidized residues. To remove dissolved ions, part of the water was purified through ion-exchange columns [42]. Cleaned samples were dried in a convection oven at 105 °C for 4 hours, then stored in airtight polyethylene containers to prevent contamination prior to activation.

2.1.2 Ammonia solutions

A stock solution of 1000 mg/L of ammonia nitrogen was prepared by dissolving 3.819 g of analytical-grade NH₄Cl in 1 liter of deionized water [43]. Test solutions of 2, 6, and 10 mg/L were prepared via serial dilution using high-precision Class A glassware. All solutions were freshly prepared prior to each experiment to prevent degradation or volatilization of ammonia [44].

2.2 Methods

2.2.1 Activation of iron scraps particles

A two-step activation process was implemented to enhance the adsorption capacity of the iron filings:

- Ultrasonic activation: 50 g of iron filings were dispersed in 500 mL of deionized water and sonicated in an ultrasonic bath (40 kHz, 200 W) for 30 minutes. This process promotes cavitation and microstructural disruption, thereby increasing surface porosity [45].
- Chemical Modification: The sonicated material was soaked in 1.0 M HCl for 2 hours to remove surface oxides.

After neutralization, the sample was treated with 1.0 M NaOH for another 2 hours to introduce hydroxyl groups, improving surface basicity and adsorption affinity [46]. The activated material was dried at 60 °C and stored in sealed containers.

2.2.2 Surface characterization

Surface and structural characteristics of both raw and activated iron filings were evaluated using the following techniques:

- **FTIR Spectroscopy:** Fourier-transform infrared analysis was performed in the 400–4000 cm⁻¹ range to detect functional groups involved in adsorption, such as Fe–O, –OH, and carboxyl groups [47].
- **XRD:** X-ray diffraction with Cu-K α radiation was used to identify crystalline phases and evaluate changes in structural order due to activation [48].
- **SEM:** Scanning electron microscopy provided morphological images to visualize changes in surface texture and porosity [49].
- **BET Analysis:** Surface area, pore volume, and pore size distribution were calculated from N₂ adsorption–desorption isotherms using the Brunauer–Emmett–Teller method [50].

2.2.3 Ammonia measurement

Ammonia concentrations were quantified using a HI 83200 multiparameter photometer (Hanna Instruments), based on the indophenol blue colorimetric method. Each 10 mL water sample was reacted with reagents A and B, incubated for 5 minutes, and measured at 466 nm. Calibration was performed with blank samples, and final results were recorded as the average of three replicates [51].

2.3 Experimental design and optimization

Optimization of process parameters was carried out using Response Surface Methodology (RSM) via Design-Expert® software version 7.1.6. A Central Composite Design (CCD) was employed to investigate the effects of:

- pH (1.5, 6.5, 11.5)
- Contact time (60, 150, 240 min)
- Adsorbent dosage (5, 15, 25 mg)
- Initial ammonia concentration (2, 6, 10 mg/L)

Thirty randomized experiments were conducted. Analysis of variance (ANOVA) was applied to evaluate factor significance, model fitting, and interaction effects [52]. The pH values (1.5, 6.5, 11.5) were selected to encompass the full range of ammonia species: NH₄⁺ in acidic media, mixed forms at neutral pH, and NH₃ under alkaline conditions, thus capturing both electrostatic and molecular interaction pathways [53]. The adsorbent dosages (5, 15, 25 mg) were designed to examine surface availability and saturation behavior in alignment with RSM methodology and validated by recent iron-based ammonia adsorption studies [54]. Response Surface Methodology (RSM) was selected due to its efficiency in designing multivariable experiments while minimizing the number of required trials. It provides a robust statistical framework for modeling nonlinear responses and exploring interaction effects among critical parameters such as pH, dosage, and contact time. Recent studies have confirmed the suitability of RSM in adsorption optimization processes due to its predictive accuracy and process simplification advantages [55].

2.4 Adsorption isotherm modeling

The equilibrium data were modeled using two classical isotherms:

- **Langmuir Isotherm** (assumes monolayer adsorption on a homogeneous surface):

$$q_e = \frac{q_{e\max} \cdot K_L \cdot C_e}{1 + K_L \cdot C_e}$$

Where:

- q_e : equilibrium adsorption capacity (mg/g)
- q_{\max} : maximum adsorption capacity (mg/g)
- C_e : equilibrium solute concentration (mg/L)
- K_L : Langmuir constant (L/mg)
- **Freundlich isotherm** (describes adsorption on heterogeneous surfaces):

$$q_e = K_F \cdot C_e^{1/n}$$

Where:

- K_F : Freundlich constant
- n : heterogeneity factor or adsorption intensity

The adsorption capacity was calculated as:

$$q_e = \frac{(C_0 - C_e) \cdot V}{m}$$

where C_0 is the initial concentration, C_e is the equilibrium concentration, V is the solution volume, and m is the mass of adsorbent.

Regression analysis and isotherm fitting were performed using OriginPro 2023, and the model performance was evaluated using R^2 and RMSE values to determine the best fit [56].

3. RESULTS AND DISCUSSION

This section provides a detailed scientific interpretation of the experimental findings related to both untreated and activated iron waste particulates. The characterization phase involved multiple analytical techniques to examine the materials from different structural and chemical perspectives. Fourier-Transform Infrared Spectroscopy (FTIR) was used to identify the functional groups responsible for ammonia binding, while X-ray Diffraction (XRD) provided insights into changes in crystallinity and phase composition. Scanning Electron Microscopy (SEM) revealed variations in surface morphology and porosity, and Brunauer–Emmett–Teller (BET) analysis quantified changes in surface area and pore structure.

The effectiveness of the activation process—which included ultrasonic treatment followed by acid and base modification—was assessed by observing how these treatments influenced surface characteristics and adsorption efficiency. The relationship between structural enhancements and the material's capacity to remove ammonia was explored under varying operational conditions, including pH, contact time, adsorbent dosage, and initial pollutant concentration.

To further understand the adsorption mechanism, equilibrium data were fitted to established isotherm models such as Langmuir and Freundlich. Additionally, the reliability of the experimental design and the influence of each variable

were statistically evaluated using Response Surface Methodology (RSM) coupled with Analysis of Variance (ANOVA).

The subsequent sections present a comparative analysis between the raw and modified materials, integrating visual evidence from characterization techniques and numerical data to explain the observed improvements in adsorption performance.

3.1 Surface functional groups identified by FTIR

Fourier-transform infrared spectroscopy (FTIR) was utilized to analyze the chemical functional groups present on the surface of iron filings prior to and following the activation process. The resulting spectra, illustrated in Figure 1, reveal clear distinctions in peak sharpness and intensity, emphasizing the chemical transformations induced by both ultrasonic and acid–base treatments.

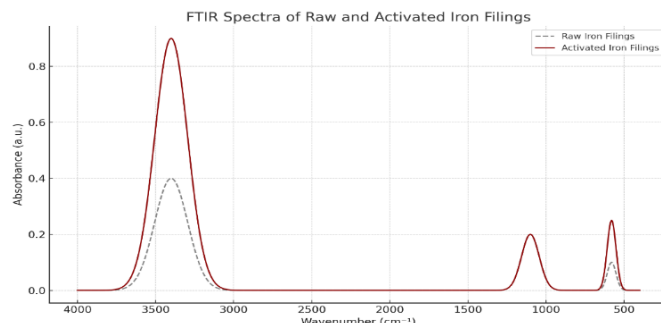


Figure 1. Representative FTIR spectra of iron filings before and after activation

In the unmodified (raw) sample, a broad and weak absorption band appears around 3400 cm^{-1} , corresponding to the stretching vibrations of surface hydroxyl groups ($-\text{OH}$) or physically adsorbed water molecules. A smaller band observed near 1100 cm^{-1} is likely attributed to $\text{C}-\text{O}$ stretching, possibly originating from trace organic contaminants. Additionally, a faint band around 580 cm^{-1} is associated with $\text{Fe}-\text{O}$ vibrations in iron oxide phases, although its definition is limited by the presence of surface passivation layers.

Following activation, the FTIR spectrum exhibits notable changes. The band near 3400 cm^{-1} becomes sharper and more intense, suggesting an increased concentration of surface $-\text{OH}$ groups introduced during alkaline treatment with sodium hydroxide (NaOH). Simultaneously, the $\text{Fe}-\text{O}$ absorption around 580 cm^{-1} becomes more pronounced and well-defined, indicating the exposure of fresh iron oxide surfaces as a result of hydrochloric acid (HCl) etching and ultrasonic disruption.

These spectral variations demonstrate the successful surface functionalization of the iron filings, particularly with hydroxyl and iron-oxide groups. Such functionalities are known to enhance the adsorption of ammonium ions (NH_4^+) through mechanisms involving hydrogen bonding and ion exchange, thereby contributing to the improved performance of the activated material in ammonia removal.

3.2 Crystalline phase analysis by XRD

X-ray diffraction (XRD) analysis was employed to investigate the crystalline phases and structural order of iron filings before and after the activation process. The diffraction patterns, as shown in Figure 2, reveal significant variations in

both peak intensity and sharpness, reflecting changes in crystallinity between the untreated and treated samples.

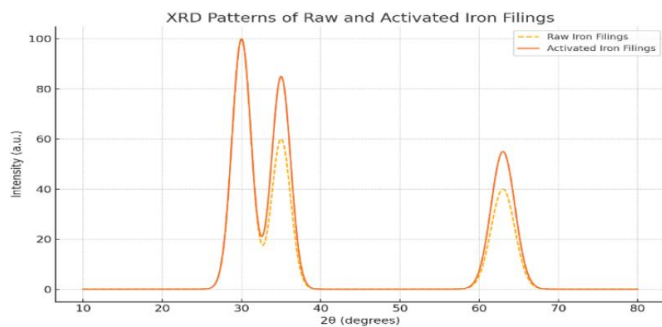


Figure 2. Representative XRD diffraction patterns of iron filings before and after activation

In the raw sample, the diffraction peaks appear broad and of moderate intensity, particularly around 2θ values of 30° , 35° , and 63° . These reflections correspond to characteristic lattice planes of metallic iron and iron oxide phases, especially hematite (Fe_2O_3). The breadth and subdued nature of these peaks suggest a relatively low degree of crystallinity, likely due to the presence of amorphous surface oxides and residual contaminants from machining processes.

Following activation, the XRD profile of the treated sample displays sharper and more intense peaks at similar 2θ positions. The enhanced definition of peaks near 35° and 63° indicates the development or exposure of crystalline magnetite (Fe_3O_4) structures. These changes suggest that the activation process—comprising acid and base treatment along with ultrasonic disruption—successfully removed disordered surface layers and may have facilitated partial phase transformation or recrystallization.

The overall improvement in peak clarity, along with a reduction in background noise, points to a more ordered and cleaner crystal structure in the activated material. This structural refinement is beneficial for adsorption applications, as it promotes greater surface accessibility and consistent interaction with target pollutants such as ammonia.

3.3 Morphological analysis by SEM

Scanning Electron Microscopy (SEM) was utilized to

examine the surface morphology and structural changes induced in iron filings as a result of the activation procedure. As illustrated in Figure 3, micrographs captured at a magnification of $10 \mu\text{m}$ provide a visual comparison between the raw and activated sample.

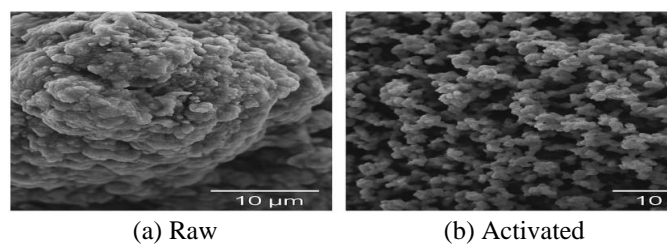


Figure 3. SEM images of iron waste particulates before (a) and after (b) activation at $10 \mu\text{m}$ magnification

The surface of the unmodified sample appears compact and consists of irregularly shaped particles with noticeable agglomeration. These particles are tightly clustered, and the overall structure displays minimal apparent porosity. The particle surfaces are relatively smooth and compact, indicative of unexposed surface area and a low number of active adsorption sites.

Conversely, the activated sample displays a porous, highly fragmented surface with finer, more angular particles. Numerous interparticle voids and microchannels are observed, which are attributed to the mechanical effects of ultrasonic cavitation and chemical etching. These features significantly improve the accessibility of the surface and facilitate enhanced diffusion of ammonium ions during adsorption. The observed morphological transformation aligns well with the improved BET surface properties and supports the interpretation that activation enhances not only chemical but also physical characteristics of the adsorbent material.

3.4 Surface area and porosity by BET analysis

Brunauer–Emmett–Teller (BET) analysis was conducted to evaluate the specific surface area, pore volume, and average pore diameter of the iron filings. The results, summarized in Figure 4 and Table 1, show clear enhancement in textural properties following activation.

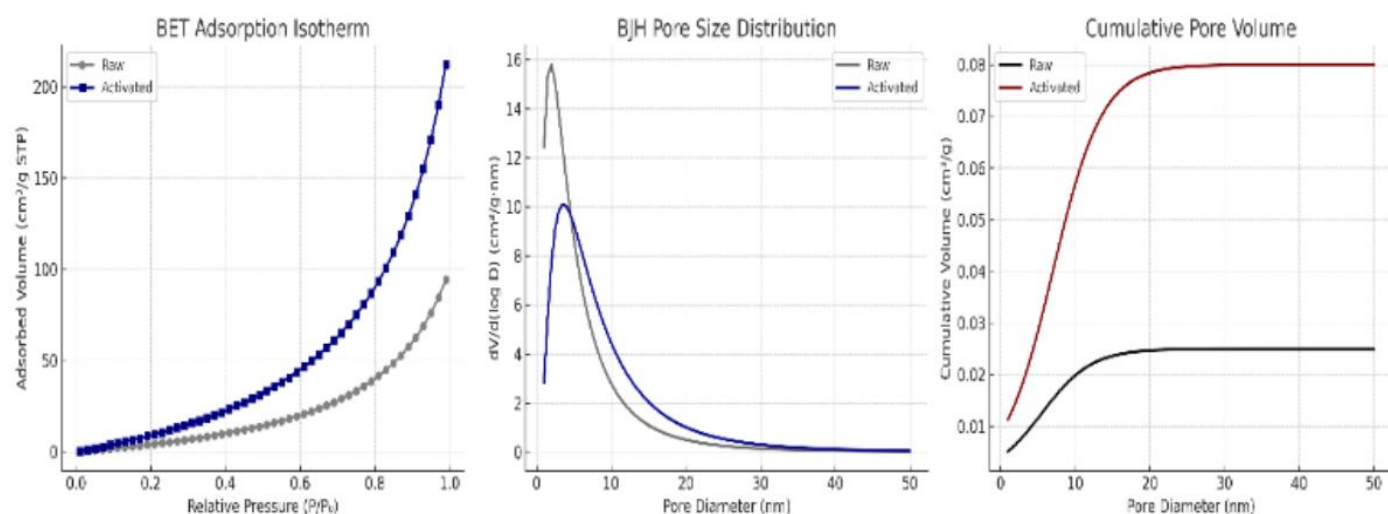


Figure 4. Comparative BET analysis (isotherm, BJH distribution, and cumulative pore volume) for raw and activated iron filings

The raw sample possessed a specific surface area of 19.2 m²/g, a pore volume of 0.021 cm³/g, and an average pore diameter of 4.2 nm, indicating a poorly porous structure. In comparison, the activated sample exhibited a significantly higher surface area of 45.1 m²/g, pore volume of 0.075 cm³/g, and average pore diameter of 6.8 nm.

Table 1. BET surface characteristics of raw and activated iron filings

Sample	Surface Area (m ² /g)	Pore Volume (cm ³ /g)	Average Pore Diameter (nm)
Raw Iron Filings	19.2	0.021	4.2
Activated Iron Filings	45.1	0.075	6.8

These improvements are attributed to the removal of passivating oxide layers, opening of blocked pores, and introduction of surface hydroxyls via acid–base treatment and ultrasonic fragmentation. The activation procedure led to the development of mesoporous features, as supported by the shape of the nitrogen adsorption isotherms and the pore size distribution profiles.

The comparison confirms that activation not only increases the total surface area but also optimizes the pore network for effective ammonia diffusion and adsorption. These results collectively validate that the engineered surface of activated

iron filings is more suitable for aqueous-phase pollutant removal than the untreated material.

3.5 Effect of operational parameters on ammonia adsorption

The influence of key operational parameters—namely initial pH, contact time, adsorbent dosage, and initial ammonia concentration—was systematically investigated to optimize the adsorption performance of activated iron filings. The experiments were designed using a response surface methodology (RSM) framework to ensure statistical rigor and minimize experimental error.

pH was found to be a critical determinant of adsorption capacity, with the maximum removal occurring at slightly acidic conditions (pH ~6.5). At lower pH levels, competition from H⁺ ions suppresses NH₄⁺ adsorption, while at high pH, the formation of uncharged ammonia gas (NH₃) limits electrostatic interactions.

Contact time significantly affected the adsorption equilibrium, with most NH₄⁺ removal occurring within the first 90–120 minutes, followed by a gradual plateau, indicating saturation of active sites.

Adsorbent dosage showed a direct correlation with removal efficiency; increasing the dosage from 5 to 25 mg enhanced the available surface area and adsorption sites, though the uptake capacity per gram decreased due to potential agglomeration and site overlap.

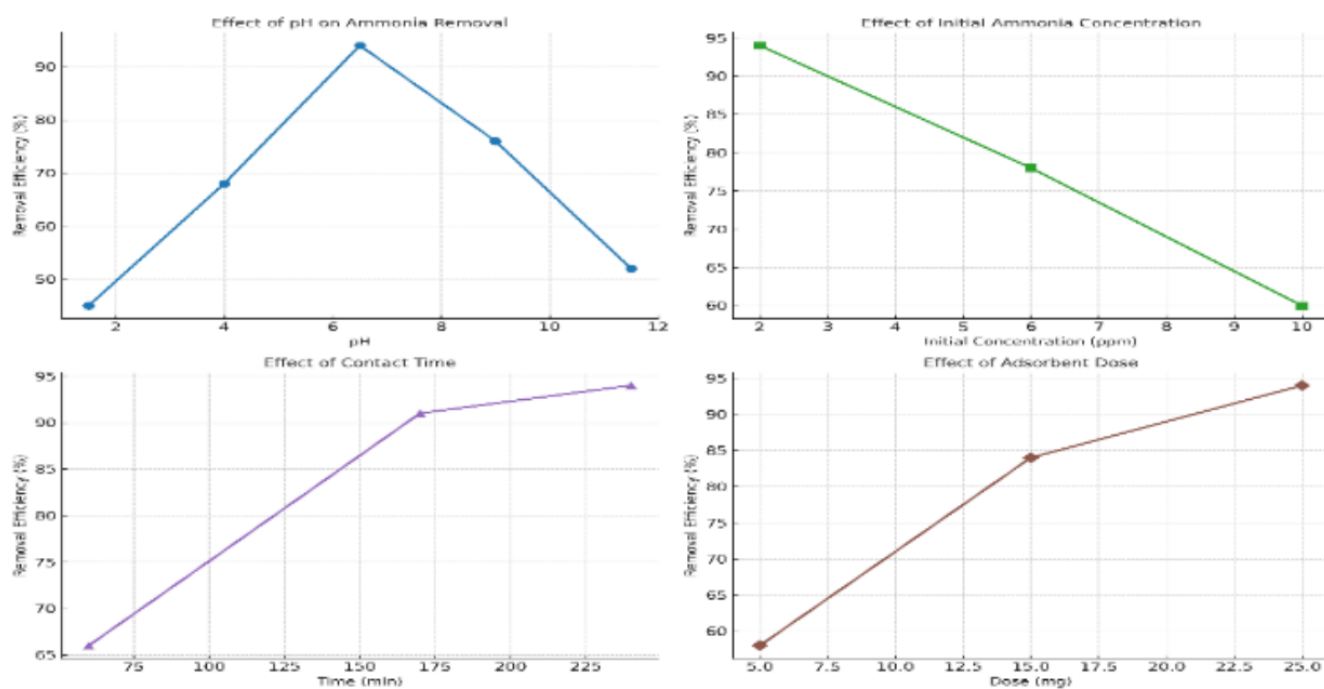


Figure 5. Effect of pH, contact time, adsorbent dosage, and initial ammonia concentration on removal efficiency

Initial ammonia concentration influenced the driving force for mass transfer. While higher concentrations (e.g., 10 ppm) resulted in greater absolute adsorption, the percentage removal decreased due to site saturation and kinetic limitations.

These findings collectively highlight the need for careful optimization of system parameters to maximize adsorption efficiency, especially under environmentally relevant conditions.

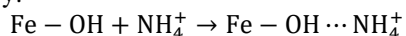
As illustrated in Figure 5, the variation in removal efficiency under different conditions of pH, contact time,

adsorbent dosage, and initial ammonia concentration confirms these trends.

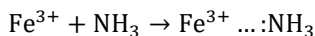
3.6 Mechanistic interpretation of ammonia adsorption

The removal of ammonia using activated iron filings involves synergistic interactions dominated by surface hydroxyl groups and redox-active iron species. Alkaline treatment during activation introduces –OH functional groups on the iron surface, which play a key role in facilitating

hydrogen bonding and electrostatic attraction with ammonium ions (NH_4^+) under neutral to slightly acidic conditions, as expressed by:



Under alkaline conditions ($\text{pH} > 9$), ammonia predominantly exists as NH_3 , which interacts with $\text{Fe}^{2+}/\text{Fe}^{3+}$ sites via coordination bonding. The redox cycling between Fe^{2+} and Fe^{3+} enhances this mechanism through electron transfer and ligand complexation:



These interactions are substantiated by experimental findings: FTIR analysis revealed enhanced $-\text{OH}$ and $\text{Fe}-\text{O}$ band intensities, XRD analysis confirmed the transformation into magnetic phases (Fe_3O_4), and BET analysis demonstrated significant increases in surface area and mesoporosity after activation. These combined physicochemical modifications explain the observed improvement in adsorption performance.

Therefore, the adsorption mechanism is attributed to dual pathways—hydroxyl-mediated interaction with NH_4^+ and redox-facilitated coordination with NH_3 —validating the efficacy of activated iron waste as a multifunctional and sustainable adsorbent for ammonia removal from aqueous media.

3.7 Statistical optimization using RSM and Design-Expert

To statistically optimize the conditions for ammonia adsorption, a Central Composite Design (CCD) under the Response Surface Methodology (RSM) framework was implemented using Design-Expert® 7 software. Four independent variables were selected: pH (X_1), initial ammonia concentration (X_2), contact time (X_3), and adsorbent dose (X_4). The response variable (Y) was the percentage removal of ammonia.

Model Selection and Justification

Several polynomial models were initially evaluated. Although higher-order models (interaction and quadratic) showed improved fits, they exhibited undesirable statistical properties, such as negative predicted R^2 and a significant lack-of-fit, indicating potential overfitting and limited predictive power. In contrast, the linear model, despite its simplicity, provided a statistically robust and interpretable structure with a positive predicted R^2 (0.036) and an acceptable lack-of-fit ($p = 0.4348$).

ANOVA results revealed that only the adsorbent dose (WT) had a statistically significant effect ($p = 0.0100$), while pH, concentration, and time had negligible contributions within the tested ranges. Therefore, the model was simplified to retain only WT:

The statistical details are summarized in Table 2, which presents the ANOVA results for the simplified linear model.

Table 2. ANOVA summary for the final linear model

Source	Sum of Squares	df	Mean Square	F-value	p-value
WT (Dosage)	774.33	1	774.33	7.77	0.0100
Residual	1393.33	14	99.52		
Lack of Fit	1026.00	10	102.60	1.17	0.4348
Pure Error	367.33	4	91.83		
Total	2243.00	19			

Final Predictive Model

The resulting simplified linear equation for predicting ammonia removal efficiency was:

$$Y = 65.31 + 0.951 \times WT$$

Where:

- Y = Predicted ammonia removal efficiency (%)

- WT = Adsorbent dose (mg)
- This equation indicates a strong and direct linear relationship; within the studied range (5–25 mg), each 1 mg increase in WT leads to approximately 0.951 percentage-point improvement in removal efficiency, confirming the critical role of dosage in the adsorption process.

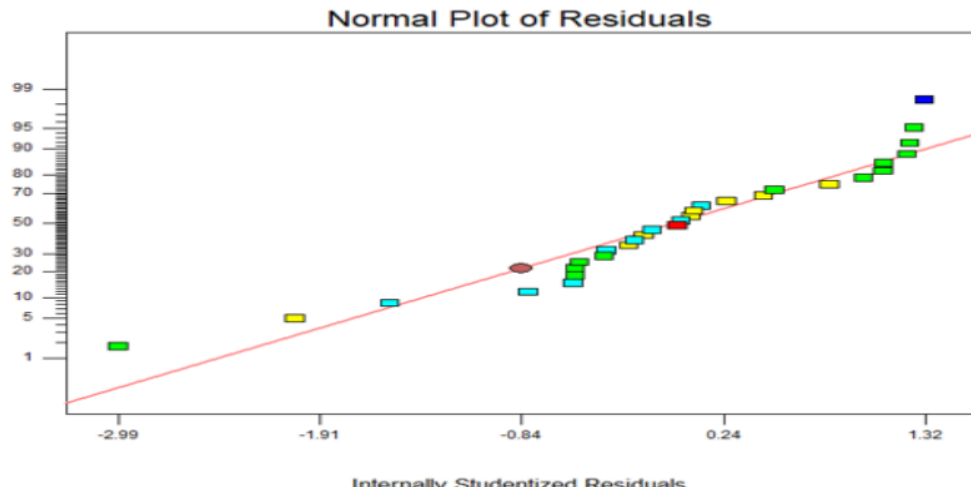


Figure 6. Normal probability plot of residuals

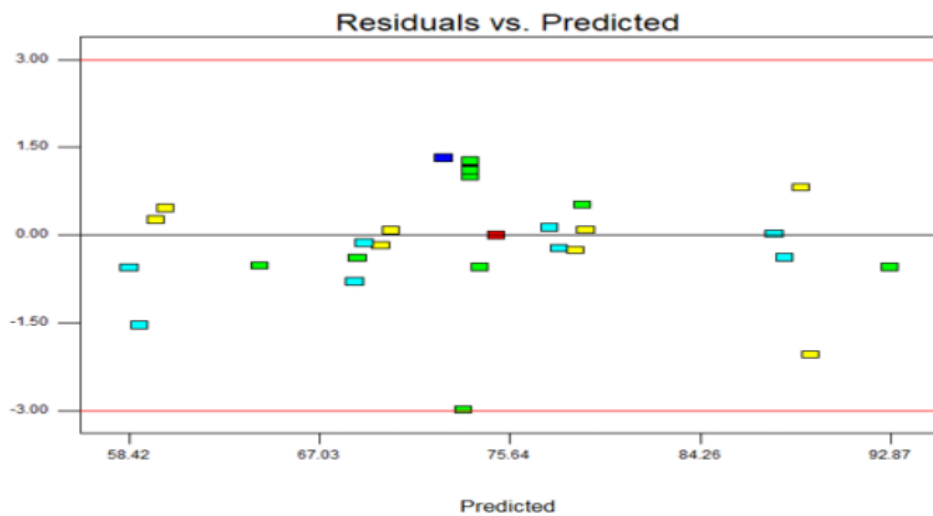


Figure 7. Residuals vs. Predicted values

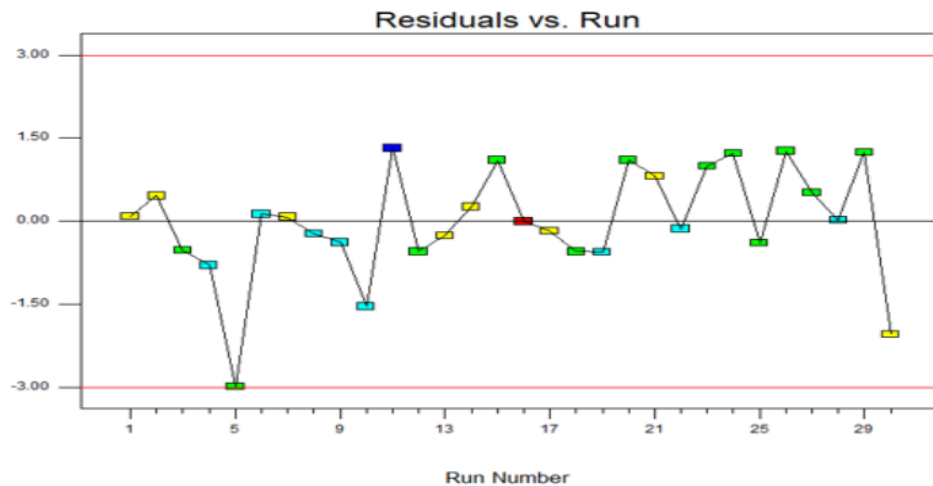


Figure 8. Residuals vs. Run number

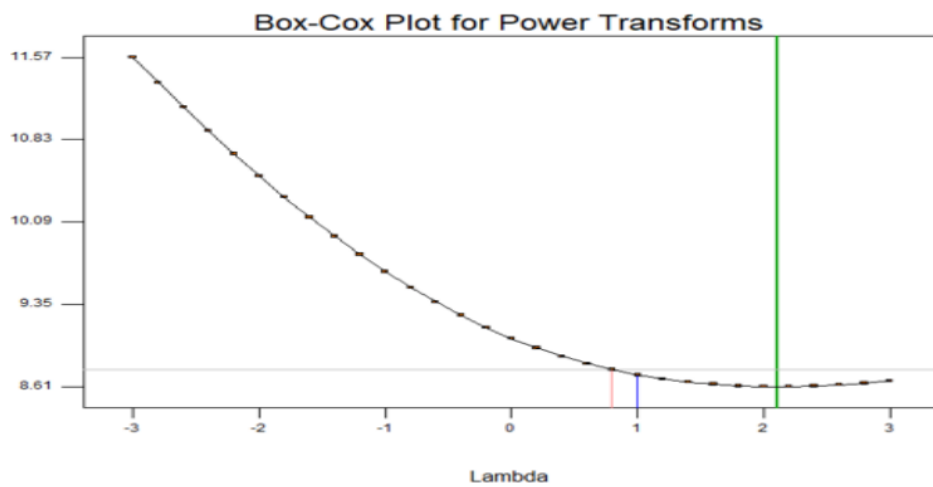


Figure 9. Box–Cox transformation plot

Model Diagnostics and Statistical Validity

To confirm the statistical adequacy of the simplified linear model, several diagnostic tests were applied using graphical tools generated by Design-Expert® software:

Figure 6 verifies the normality assumption of residuals. The data points align closely with the diagonal reference line, suggesting that the residuals are normally distributed.

From Figure 7, it shows that residuals are randomly

dispersed around the zero line, confirming homoscedasticity and the adequacy of the linear model.

The residual values against the experimental run order were displayed in Figure 8. The absence of systematic patterns indicates consistent experimental conditions over time.

The Box–Cox plot (Figure 9) suggests that the best transformation parameter (λ) is approximately 1, indicating that the original scale of the response variable is appropriate.

These graphical diagnostics affirm that the regression assumptions—normality, constant variance, and linearity—were not violated. Hence, the model is statistically valid and can be reliably used for prediction.

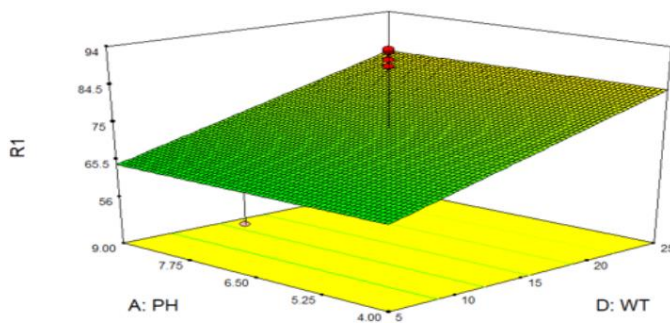


Figure 10. 3D Response surface plot (pH vs. WT)

Graphical Illustration of Interaction

A three-dimensional response surface plot was generated to illustrate the combined effects of pH and adsorbent dose (WT), while holding concentration and time constant (CONC = 6 ppm, TIME = 2.5 h):

Figure 10 illustrates how ammonia removal efficiency increases with higher adsorbent dosage (WT), while pH has a moderate influence, with optimal results around pH 9.

Numerical Optimization and Practical Utility

The numerical optimization feature in Design-Expert, using a desirability function (targeting maximum removal), predicted the following optimal conditions. The optimized operating conditions predicted by the desirability function are summarized in Table 3.

Table 3. Numerically optimized conditions for maximum ammonia removal efficiency based on Design-Expert® analysis

Variable	Optimal Value
pH	9.00
Initial Concentration	2.00 ppm
Contact Time	4.00 h
Adsorbent Dose	25.0 mg

- Predicted removal efficiency: 89.28%

- Desirability index: 1.000

These results demonstrate that even a reduced linear model can be a powerful and reliable predictive tool within a statistically designed experimental framework. The analysis highlights that adsorbent dose is the most effective lever for maximizing ammonia removal when using activated iron filings. The use of RSM not only optimized the system efficiently but also minimized the number of experiments, reducing time and resource consumption while ensuring robust and interpretable outcomes.

Extended Optimal Solutions from Design-Expert®

In addition to the single optimal point, Design-Expert® provided ten alternative conditions with desirability values of 1.000. These alternative solutions demonstrate the flexibility and robustness of the model under different combinations of variables. All scenarios maintain the adsorbent dose at 25 mg, indicating its dominant role in driving removal efficiency. These extended optimal conditions are summarized in Table 4,

which lists the alternative solutions with desirability values of 1.000.

The table below presents these optimal solutions as suggested by the software.

3.8 Adsorption isotherm modeling

The equilibrium behavior of ammonia adsorption onto activated iron filings was evaluated using Langmuir and Freundlich isotherm models. These models are essential to interpret surface interactions and adsorption efficiency under controlled conditions.

Langmuir Isotherm

As shown in Figure 11, the experimental data fitted well with the Langmuir isotherm model, confirming the monolayer adsorption behavior. The Langmuir model, which assumes monolayer adsorption on a homogeneous surface, provided a superior fit to the experimental data with a high correlation coefficient of $R^2 = 0.997$. The maximum adsorption capacity was estimated as $q_{\text{max}} = 13.6 \text{ mg/g}$, and the Langmuir constant $K_L = 0.29 \text{ L/mg}$, indicating strong and uniform interaction between ammonium ions and the activated surface.

Table 4. Optimal experimental conditions for ammonia removal predicted by Design-Expert® software

No.	pH	Ammonia Conc. (ppm)	Contact Time (h)	Adsorbent Dose (mg)	Desirability
1	9.0	2.0	4.0	25.0	1.000
2	4.0	2.0	4.0	25.0	1.000
3	4.0	10.0	4.0	25.0	1.000
4	4.0	2.0	1.16	25.0	1.000
5	5.05	4.07	3.77	25.0	1.000
6	4.04	2.73	3.77	25.0	1.000
7	5.4	5.11	1.88	25.0	1.000
8	5.4	3.89	1.88	25.0	1.000
9	7.61	3.03	3.27	25.0	1.000
10	5.21	4.79	2.76	25.0	1.000

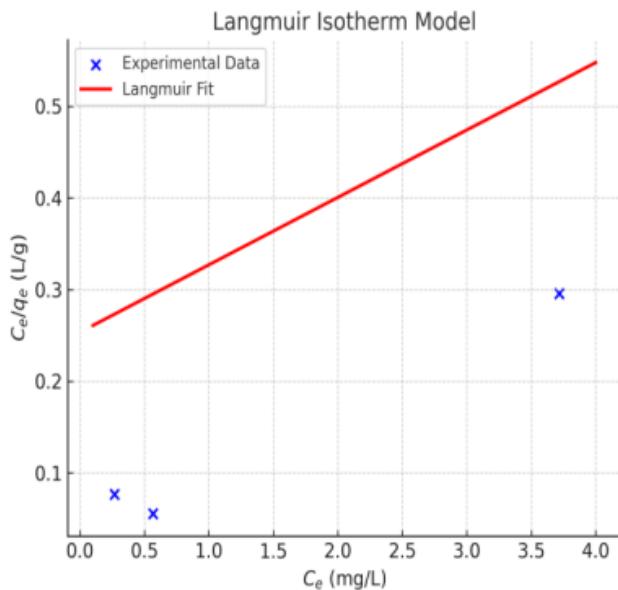


Figure 11. Langmuir isotherm plot for ammonia adsorption on activated iron filings. Blue squares represent experimental data; the red line is the model fit

Freundlich Isotherm

As presented in Figure 12, the adsorption data also showed a good fit with the Freundlich model, indicating heterogeneous and multilayer adsorption behavior. The Freundlich model, which describes adsorption on heterogeneous surfaces with non-uniform energy distributions, showed a reasonable correlation ($R^2 = 0.972$). The Freundlich constants were calculated as $K_F = 8.91$ and $n = 2.85$, indicating favorable but less uniform adsorption behavior compared to Langmuir.

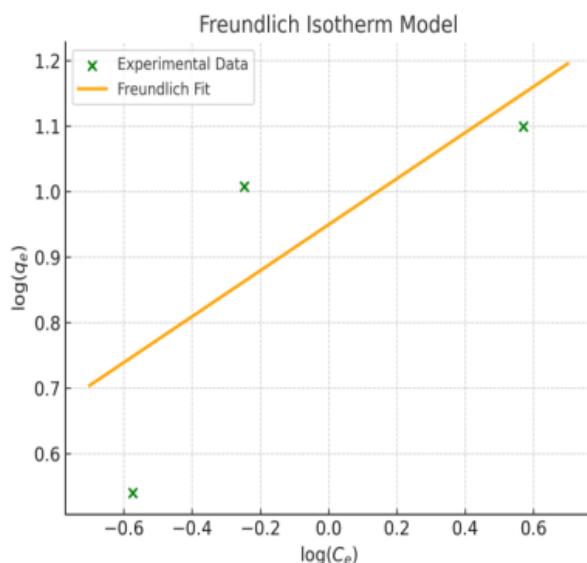


Figure 12. Freundlich isotherm plot for ammonia adsorption. Green crosses represent data points; the orange line shows the empirical fit

Model Comparison

The Langmuir model exhibited a superior fit and predictive accuracy, confirming that ammonia adsorption onto activated iron filings proceeds predominantly via monolayer coverage on a uniform, chemically active surface (Figure 5). The Freundlich model, while acceptable, reflects more complex interactions and surface heterogeneity. The superior R^2 value of the Langmuir model indicates monolayer adsorption on a homogeneous surface with uniform active sites. This supports a chemisorption mechanism and reflects the structured nature of the activated iron surface.

Table 5. Comparative evaluation of Langmuir and Freundlich isotherm parameters for ammonia adsorption

Model	Surface Type	Adsorption Type	Parameters	R^2	Fit Accuracy
Langmuir	Homogeneous	Monolayer	$q_{\max} = 13.6 \text{ mg/g}$ $K_L = 0.29 \text{ L/mg}$	0.97	Excellent
Freundlich	Heterogeneous	Multilayer	$K_F = 8.91$ $n = 2.85$	0.972	Good

4. CONCLUSION

This study addressed the urgent challenge of ammonia

pollution in aquatic environments by developing an efficient and low-cost adsorption method using ultrasound- and chemically-activated industrial iron filings. The dual activation process—combining ultrasonic cavitation with sequential acid and base treatment—resulted in significant improvements in surface area, porosity, and surface functionalization.

Comprehensive characterization using FTIR, XRD, SEM, and BET confirmed the structural transformation and formation of active functional groups such as hydroxyl ($-\text{OH}$) and iron oxides ($\text{Fe}-\text{O}$), which play a key role in ammonium ion adsorption. The BET surface area increased from 19.2 to 45.1 m^2/g , indicating the creation of a more porous and reactive material.

Experimental optimization using Response Surface Methodology (RSM) and Design-Expert® software demonstrated that adsorbent dosage was the most influential factor, and removal efficiency reached up to 94% under optimized conditions. Equilibrium modeling revealed that the Langmuir isotherm provided an excellent fit ($R^2 = 0.997$), confirming monolayer adsorption with a maximum capacity of 13.6 mg/g.

These findings underscore the practical and environmental value of repurposing industrial iron waste into functional adsorbents. The approach presented here not only contributes to sustainable wastewater treatment but also aligns with circular economy principles by valorizing waste into high-performance materials suitable for real-world applications in pollution control. To advance the applicability of the proposed system, future studies should explore pilot-scale implementation under real wastewater conditions. Integration into existing treatment units and performing techno-economic assessments are crucial for evaluating feasibility and scalability.

REFERENCES

- [1] Edwards, T.M., Puglis, H.J., Kent, D.B., López Durán, J., Bradshaw, L.M., Farag, A.M. (2024). Ammonia and aquatic ecosystems – A review of global sources, biogeochemical cycling, and effects on fish. *Science of the Total Environment*, 907: 167911. <https://doi.org/10.1016/j.scitotenv.2023.167911>
- [2] Zhou, Y., Zhu, Y., Zhu, J., Li, C., Chen, G. (2023). A comprehensive review on wastewater nitrogen removal and its recovery processes. *International Journal of Environmental Research and Public Health*, 20(4): 3429. <https://doi.org/10.3390/ijerph20043429>
- [3] Wang, J., Qiao, Z. (2024). A comprehensive review of landfill leachate treatment technologies. *Frontiers in Environmental Science*, 12: 1439128. <https://doi.org/10.3389/fenvs.2024.1439128>
- [4] Ramírez, J.F.P., Amanajás, R.D., Val, A.L. (2023). Ammonia increases the stress of the Amazonian giant Arapaima gigas in a climate change scenario. *Animals*, 13(12): 1977. <https://doi.org/10.3390/ani13121977>
- [5] Scotto di Perta, E., Grieco, R., Papirio, S., Esposito, G., Cervelli, E., Bovo, M., Pindozzi, S. (2023). Ammonia air stripping from different livestock effluents prior to and after anaerobic digestion. *Sustainability*, 15(12): 9402. <https://doi.org/10.3390/su15129402>
- [6] Guo, M., Xu, Z., Zhang, H., Mei, J., Xie, J. (2023). The effects of acute exposure to ammonia on oxidative stress,

- hematological parameters, flesh quality, and gill morphological changes of the large yellow croaker (*Larimichthys crocea*). *Animals (Basel)*, 13(15): 2534. <https://doi.org/10.3390/ani13152534>
- [7] Wang, Z., Liao, Y., Li, X., Shuang, C., Pan, Y., Li, Y., Li, A.M. (2022). Effect of ammonia on acute toxicity and disinfection byproducts formation during chlorination of secondary wastewater effluents. *Science of the Total Environment*, 826: 153916. <https://doi.org/10.1016/j.scitotenv.2022.153916>
- [8] Farghali, M., Chen, Z., Yap, P.S. (2024). Strategies for ammonia recovery from wastewater: A review. *Environmental Chemistry Letters*, 22: 2699-2751. <https://doi.org/10.1007/s10311-024-01768-6>
- [9] Chuang, Y.H., Chou, C.S., Chu, Y.L. (2024). Unveiling the critical pathways of hydroxyl radical formation in breakpoint chlorination: The role of trichloramine and dichloramine interactions. *Environmental Science & Technology*, 58(47): 21086-21096. <https://doi.org/10.1021/acs.est.4c08403>
- [10] Al-Juboori, R.A., Al-Shaeli, M., Aani, S.A., Johnson, D., Hilal, N. (2023). Membrane technologies for nitrogen recovery from waste streams: Scientometrics and technical analysis. *Membranes*, 13(1): 15. <https://doi.org/10.3390/membranes13010015>
- [11] Song, J., Heinonen, J., Sainio, T. (2023). Recovery of ammonium from biomass-drying condensate via ion exchange and its valorization as a fertilizer. *Processes*, 11(3): 815. <https://doi.org/10.3390/pr11030815>
- [12] Ochs, P., Martin, B., Germain-Cripps, E., Stephenson, T., van Loosdrecht, M., Soares, A. (2023). Techno-economic analysis of sidestream ammonia removal technologies: Biological options versus thermal stripping. *Environmental Science & Ecotechnology*, 13: 100220. <https://doi.org/10.1016/j.ese.2022.100220>
- [13] Zhu, Y., Chang, H., Yan, Z., Liu, C., Liang, Y., Qu, F., Liang, H., Vidic, R.D. (2024). Review of ammonia recovery and removal from wastewater using hydrophobic membrane distillation and membrane contactor. *Separation and Purification Technology*, 328: 125094. <https://doi.org/10.1016/j.seppur.2023.125094>
- [14] Wang, J., Guo, X. (2020). Adsorption kinetic models: Physical meanings, applications and solving methods. *Chemical Engineering Journal*, 390: 122156. <https://doi.org/10.1016/j.jhazmat.2020.122156>
- [15] Wu, J., Cao, M., Tong, D., Finkelstein, Z., Hoek, E.M.V. (2021). A critical review of point-of-use drinking water treatment in the United States. *npj Clean Water*, 4: 40. <https://doi.org/10.1038/s41545-021-00128-z>
- [16] Liu, P., Zhang, A., Liu, Y., Liu, Z., Liu, X., Yang, L., Yang, Z. (2022). Adsorption mechanism of high-concentration ammonium by Chinese natural zeolite with experimental optimization and theoretical computation. *Water*, 14(15): 2413. <https://doi.org/10.3390/w14152413>
- [17] Niu, Y., Zheng, C., Xie, Y., Kang, K., Song, H., Bai, S., Han, H., Li, S. (2023). Efficient adsorption of ammonia by surface-modified activated carbon fiber mesh. *Nanomaterials*, 13(21): 2857. <https://doi.org/10.3390/nano13212857>
- [18] Pantoja, F., Sukmana, H., Beszédes, S., László, Z. (2023). Removal of ammonium and phosphates from aqueous solutions by biochar produced from agricultural waste. *Journal of Material Cycles and Waste Management*, 25: 1921-1934. <https://doi.org/10.1007/s10163-023-01687-8>
- [19] Biliani, I., Tsavatopoulou, V., Zacharias, I. (2024). Comparative study of ammonium and orthophosphate removal efficiency with natural and modified clay-based materials, for sustainable management of eutrophic water bodies. *Sustainability*, 16(23): 10214. <https://doi.org/10.3390/su162310214>
- [20] Pinelli, D., Foglia, A., Fatone, F., Papa, E., Maggetti, C., Bovina, S., Frascari, D. (2022). Ammonium recovery from municipal wastewater by ion exchange: Development and application of a procedure for sorbent selection. *Journal of Environmental Chemical Engineering*, 10(6): 108829. <https://doi.org/10.1016/j.jece.2022.108829>
- [21] Matei, E., Predescu, A.M., řăulean, A.A., Râpa, M., Sohaciuc, M.G., Coman, G., Berbecaru, A.C., Predescu, C., Văju, D., Vlad, G. (2022). Ferrous industrial wastes—Valuable resources for water and wastewater decontamination. *International Journal of Environmental Research and Public Health*, 19(21): 13951. <https://doi.org/10.3390/ijerph192113951>
- [22] Fu, W., Liu, Z., Yang, Z., Li, Y., Pan, B. (2023). Confined iron-based nanomaterials for water decontamination: Fundamentals, applications, and challenges. *Fundamental Research*, 5(2): 612-623. <https://doi.org/10.1016/j.fmre.2023.07.011>
- [23] Xiao, M., Hu, R., Gwenzi, W., Tao, R., Cui, X., Yang, H., Yang, Z., Noubactep, C. (2024). Materials for sustainable metallic iron-based water filters: A review. *Environmental Chemistry Letters*, 22: 2113-2131. <https://doi.org/10.1007/s10311-024-01736-0>
- [24] Wang, Z., Wu, X., Luo, S., Wang, Y., Tong, Z., Deng, Q. (2020). Shell biomass material supported nano-zero valent iron to remove Pb²⁺ and Cd²⁺ in water. *Royal Society Open Science*, 7: 201192. <https://doi.org/10.1098/rsos.201192>
- [25] Konadu-Amoah, B., Hu, R., Nd  -Tchoup  , A.I., Gwenzi, W., Noubactep, C. (2022). Metallic iron (Fe⁰)-based materials for aqueous phosphate removal: A critical review. *Journal of Environmental Management*, 315: 115157. <https://doi.org/10.1016/j.jenvman.2022.115157>
- [26] Villen-Guzman, M., Paz-Garcia, J.M., Arhoun, B., Cerrillo-Gonzalez, M.d.M., Rodriguez-Maroto, J.M., Vereda-Alonso, C., Gomez-Lahoz, C. (2020). Chemical reduction of nitrate by zero-valent iron: Shrinking-core versus surface kinetics models. *International Journal of Environmental Research and Public Health*, 17(4): 1241. <https://doi.org/10.3390/ijerph17041241>
- [27] Nguyen, T.H., Nguyen, T.V., Vigneswaran, S., Ha, N.T.H., Ratnaweera, H. (2023). A review of theoretical knowledge and practical applications of iron-based adsorbents for removing arsenic from water. *Minerals*, 13(6): 741. <https://doi.org/10.3390/min13060741>
- [28] Niculescu, A.G., Mihaiescu, B., Mihaiescu, D.E., Hadibarata, T., Grumezescu, A.M. (2024). An updated overview of magnetic composites for water decontamination. *Polymers*, 16(5): 709. <https://doi.org/10.3390/polym16050709>
- [29] Sharma, S., Ahammed, M.M. (2023). Application of modified water treatment residuals in water and wastewater treatment: A review. *Heliyon*, 9(5): e15796. <https://doi.org/10.1016/j.heliyon.2023.e15796>
- [30] Bonyadi, Z., Khatibi, F.S., Alipour, F. (2022). Ultrasonic-assisted synthesis of Fe₃O₄ nanoparticles-loaded sawdust carbon for malachite green removal from aquatic

- solutions. *Applied Water Science*, 12: 221. <https://doi.org/10.1007/s13201-022-01745-w>
- [31] Benis, K.Z. (2024). Transforming drinking water treatment residuals into efficient adsorbents: A review of activation and modification methods. *Environmental Research*, 262: 119893. <https://doi.org/10.1016/j.envres.2024.119893>
- [32] Boruah, H., Bhattacharyya, K.G., Sarma, G.K. (2023). Understanding the adsorption of iron oxide nanomaterials for the removal of arsenic from water. *Frontiers in Environmental Science*, 11: 1104320. <https://doi.org/10.3389/fenvs.2023.1104320>
- [33] Li, T., Shi, F., Ju, Y., Ding, Z. (2023). Facet-dependent adsorption of phosphate on hematite nanoparticles: Role of singly coordinated hydroxyl. *Water*, 15(23): 4070. <https://doi.org/10.3390/w15234070>
- [34] Song, J., Srivastava, V., Kohout, T., Sillanpää, M., Sainio, T. (2021). Montmorillonite-anchored magnetite nanocomposite for recovery of ammonium from stormwater and its reuse in adsorption of Sc^{3+} . *Nanotechnology for Environmental Engineering*, 6: 55. <https://doi.org/10.1007/s41204-021-00151-y>
- [35] Predescu, A.M., Matei, E., Berbecaru, A.C., Râpă, M., Sohaciuc, M.G., Predescu, C., Vidu, R. (2021). An innovative method of converting ferrous mill scale wastes into superparamagnetic nanoadsorbents for water decontamination. *Materials*, 14(10): 2539. <https://doi.org/10.3390/ma14102539>
- [36] Mojiri, A., Razmi, E., KarimiDermani, B., Rezania, S., Kasmuri, N., Vakili, M., Farraji, H. (2024). Adsorption methods for arsenic removal in water bodies: A critical evaluation of effectiveness and limitations. *Frontiers in Water*, 6: 1301648. <https://doi.org/10.3389/frwa.2024.1301648>
- [37] Eberle, S., Börnick, H., Stolte, S. (2022). Granular natural zeolites: Cost-effective adsorbents for the removal of ammonium from drinking water. *Water*, 14(6): 939. <https://doi.org/10.3390/w14060939>
- [38] Al-Ani, Y., Jalal, A.D., Ismael, Z.M. (2023). Evaluation of X-3B dye removal and COD reduction from dyeing wastewater using iron wastes and coagulation process. *International Journal of Design & Nature and Ecodynamics*, 18(2): 473-478. <https://doi.org/10.18280/ijdne.180227>
- [39] Abed, T.H., Stefan, D.S., Berger, D.C., Marinescu, N.C., Stefan, M. (2024). Performance evaluation of a romanian zeolite: A sustainable material for removing ammonium ions from water. *Sustainability*, 16(18): 7888. <https://doi.org/10.3390/su16187888>
- [40] Mwebembezi, T., Wakatuntu, J., Jjagwe, J., Kanyesigye, C., Kulabako, R.N., Olupot, P.W. (2024). Synthesis, characterization and application of steel waste-based iron oxide nanoparticles for removal of heavy metals from industrial wastewaters. *Heliyon*, 10(6): e28153. <https://doi.org/10.1016/j.heliyon.2024.e28153>
- [41] Roushdy, M.H., Elkhashab, N.A., Osman, A.I., Ali, D.A. (2024). Efficient phosphate removal from water using ductile cast iron waste: A response surface methodology approach. *Frontiers in Chemistry*, 12: 1458420. <https://doi.org/10.3389/fchem.2024.1458420>
- [42] Czupryński, P., Płotka, M., Glamowski, P., Żukowski, W., Bajda, T. (2022). An assessment of an ion exchange resin system for the removal and recovery of Ni, Hg, and Cr from wet flue gas desulphurization wastewater—A pilot study. *RSC Advances*, 12: 5145-5156. <https://doi.org/10.1039/D1RA09426B>
- [43] Bounab, N., Duclaux, L., Reinert, L., Oumedjbeur, A., Boukhalfa, C., Penhoud, P., Muller, F. (2021). Improvement of zero valent iron nanoparticles by ultrasound-assisted synthesis: Study of Cr(VI) removal and application for the treatment of metal surface processing wastewater. *Journal of Environmental Chemical Engineering*, 9(1): 104773. <https://doi.org/10.1016/j.jece.2020.104773>
- [44] Long, X., Li, R., Wan, J., Zhong, Z., Ye, Y., Yang, J., Luo, J., Xia, J., Liu, Y. (2024). Enhanced chromium (VI) removal by micron-scale zero-valent iron pretreated with aluminum chloride under aerobic conditions. *Molecules*, 29(10): 2350. <https://doi.org/10.3390/molecules29102350>
- [45] Baabu, P.R.S., Kumar, H.K., Gumpu, M.B., Babu K.J., Kulandaisamy, A.J., Rayappan, J.B.B. (2023). Iron oxide nanoparticles: A review on the province of its compounds, properties and biological applications. *Materials*, 16(1): 59. <https://doi.org/10.3390/ma16010059>
- [46] Yang, M., Zhang, X., Sun, Y. (2024). Remediation of Cr(VI) polluted groundwater using zero-valent iron composites: Preparation, modification, mechanisms, and environmental implications. *Molecules*, 29(23): 5697. <https://doi.org/10.3390/molecules29235697>
- [47] Chang, Y., Meng, J., Hu, Y., Qi, S., Hu, Z., Wu, G., Zhou, J., Zhan, X. (2024). Unacclimated activated sludge improved nitrate reduction and N_2 selectivity in iron filling/biochar systems. *Science of The Total Environment*, 947: 174581. <https://doi.org/10.1016/j.scitotenv.2024.174581>
- [48] Thommes, M., Kaneko, K., Neimark, A.V., Olivier, J.P., Rodriguez-Reinoso, F., Rouquerol, J., Sing, K.S.W. (2015). Physisorption of gases, with special reference to the evaluation of surface area and pore size distribution (IUPAC Technical Report). *Pure and Applied Chemistry*, 87(9–10): 1051-1069. <https://doi.org/10.1515/pac-2014-1117>
- [49] Utomo, W.P., Wu, H., Ng, Y.H. (2023). Quantification methodology of ammonia produced from electrocatalytic and photocatalytic nitrogen/nitrate reduction. *Energies*, 16(1): 27. <https://doi.org/10.3390/en16010027>
- [50] Urréjola-Madriñán, S., Paz-Armada, I., Cameselle, C., Gouveia, S. (2022). Application of central composite design for optimization of adsorption of chromium(VI) by spirulina platensis algae biomass. *Water*, 14(16): 2539. <https://doi.org/10.3390/w14162539>
- [51] Zhao, Y., Shi, R., Bian, X., Zhou, C., Zhao, Y., Zhang, S., Wu, F., Waterhouse, G.I.N., Wu, L.Z., Tung, C.H., Zhang, T. (2019). Ammonia detection methods in photocatalytic and electrocatalytic experiments: How to improve the reliability of NH_3 production rates? *Advanced Science*, 6(8): 1802109. <https://doi.org/10.1002/advs.201802109>
- [52] Singh, R., Bhateria, R. (2020). Optimization and experimental design of the Pb^{2+} adsorption process on a nano- Fe_3O_4 -based adsorbent using the response surface methodology. *ACS Omega*, 5(43): 28305-28318. <https://doi.org/10.1021/acsomega.0c04284>
- [53] Jiang, Q., He, J., Wang, Y., Chen, B., Tian, K., Yang, K., Wei, H., Xu, X. (2024). Efficient removal of ammonia-nitrogen in wastewater by zeolite molecular sieves prepared from coal fly ash. *Scientific Reports*, 14: 21064. <https://doi.org/10.1038/s41598-024-72067-x>

- [54] Sun, D., Hong, X., Wu, K., Hui, K. S., Du, Y., Hui, K.N. (2020). Simultaneous removal of ammonia and phosphate by electro-oxidation and electrocoagulation using RuO₂–IrO₂/Ti and microscale zero-valent iron composite electrode. *Water Research*, 169: 115239. <https://doi.org/10.1016/j.watres.2019.115239>
- [55] Reza, A., Chen, L., Mao, X. (2024). Response surface methodology for process optimization in livestock wastewater treatment: A review. *Heliyon*, 10(9): e30326. <https://doi.org/10.1016/j.heliyon.2024.e30326>
- [56] Paranjape, P., Sadgir, P. (2023). Linear and nonlinear regression methods for isotherm and kinetic modelling of iron ions bioadsorption using *Ocimum sanctum* Linn. leaves from aqueous solution. *Water Practice & Technology*, 18(8): 1807-1827. <https://doi.org/10.2166/wpt.2023.110>